Generalized acoustic energy density based active noise control in single frequency diffuse sound fields

Buye Xu[a)]
Signal Processing Research, Starkey Hearing Technologies, Eden Prairie, Minnesota 55344

Scott D. Sommerfeldt
Department of Physics and Astronomy, Brigham Young University, Provo, Utah 84602

(Received 6 September 2013; revised 9 July 2014; accepted 11 July 2014)

In a diffuse sound field, prior research has established that a secondary source can theoretically achieve perfect cancellation at an error microphone in the far field of the secondary source. However, the sound pressure level is generally only reduced in a small zone around the error sensor, and at a distance half of a wavelength away from the error sensor, the averaged sound pressure level will be increased by more than 10 dB. Recently an acoustic energy quantity, referred to as the generalized acoustic energy density (GED), has been introduced. The GED is obtained by using a weighting factor in the formulation of total acoustic energy density. Different values of the weighting factor can be chosen for different applications. When minimizing the GED at the error sensor, one can adjust the weighting factor to increase the spatial extent of the "quiet zone" and to achieve a desired balance between the degree of attenuation in the quiet zone and the total energy added into the sound field. © *2014 Acoustical Society of America*. [http://dx.doi.org/10.1121/1.4892754]

PACS number(s): 43.50.Ki, 43.55.Cs, 43.55.Br [BSC] Pages: 1112–1119

I. INTRODUCTION

Active noise control (ANC) of enclosed sound fields was first studied systematically by Nelson *et al*. more than 20 years ago.[1–3] In the low frequency range (below the Schroeder frequency), it has been shown that control of the global potential energy can be achieved for resonance frequencies of an enclosure by minimizing the squared pressure response at one or multiple field locations with one or more remotely placed secondary sources. Because of the relatively large spatial fluctuations in the enclosed squared pressure field, research has been carried out to determine the optimal locations for the error sensors as well as the secondary sources.[2,4,5]

For a diffuse sound field (above the Schroeder frequency), global control is usually not feasible with remotely placed secondary sources,[1] and only local "quiet zones" can be achieved.[6–8] The average 10 dB zone of quiet, which is defined to be the region around the error sensor where the attenuation is at least 10 dB, is reported to be a sphere with a diameter of about one-tenth of a wavelength for one error sensor and one remote secondary source ANC system.[6] Effort has been carried out to increase the volume of this 10 dB quiet zone by placing the error sensor in the near-field of the secondary source.[7] In the same spirit, other control strategies involving multiple control sources minimizing acoustic pressure response as well as pressure gradient responses have also been studied.[9–11] Another type of approach to mitigate the small quiet zone issue is to utilize the virtual sensor technology, which projects the quiet zone to a remote location away from the physical error sensors to cover the space where a physical sensor cannot be placed.[11–14]

The use of total acoustic energy density (ED) as the minimization quantity has been demonstrated to yield improved performance in low modal density acoustic fields, often resulting in improved global attenuation due to the fact that ED is more spatially uniform than squared pressure and therefore provides more global information.[15,16]

Recently a new energy density quantity, referred to as generalized acoustic energy density (GED), has been introduced.[17] An additional degree of freedom is incorporated into the total acoustic energy density, and thus the quantity can be optimized for different applications. However, the complexity of measurement and computation is not increased compared to the total acoustic energy density. It has been shown that GED based active noise control can further improve the results of ED based ANC below the Schroeder frequency because the GED can be spatially more uniform than the ED for enclosed sound fields.[17] In this paper, GED will be optimized to control noise in a diffuse sound field.

This paper is organized as follows. The GED and some of its general properties will be reviewed in Sec. II. An expression for the secondary source strength to minimize the GED response will be derived in Sec. II A. In Sec. III, the zone of quiet for GED based ANC will be studied analytically. Then the analytical results will be verified by a numerical simulation in Sec. IV. In Sec. V, a modified filtered-x LMS algorithm will be introduced for GED based ANC. Finally, an experimental study will be presented in Sec. VI.

II. GED

The GED is defined as follows:[17]

$$E_{G(\alpha)} = \frac{\alpha}{2\rho_0 c^2}\hat{p}\hat{p}^* + \frac{1-\alpha}{2}\rho_0 \mathbf{v}\cdot\hat{\mathbf{v}}^*, \tag{1}$$

where $\hat{\cdot}$ denotes the frequency domain variable, α is an arbitrary real number, ρ_0 is the ambient fluid density, c is the speed of sound, and $\hat{p}$ and $\hat{\mathbf{v}}$ are the complex sound pressure

a)Author to whom correspondence should be addressed. Electronic mail: buye.xu@gmail.com

TABLE I. GED with different α values.

α	0	1/2	1
GED	E_K	$1/2E_T$[a]	E_P

[a]E_T represents the total acoustic energy density.

and particle velocity. The acoustic potential energy density E_P and kinetic energy density E_K are usually written as

$$\begin{aligned} E_P &= \frac{1}{2\rho_0 c^2}\hat{p}\hat{p}^*, \\ E_K &= \frac{1}{2}\rho_0 \hat{\mathbf{v}}\cdot\hat{\mathbf{v}}^* \\ &= \frac{1}{2}\rho_0\hat{v}_1\hat{v}_1^* + \frac{1}{2}\rho_0\hat{v}_2\hat{v}_2^* + \frac{1}{2}\rho_0\hat{v}_3\hat{v}_3^* \\ &= E_{K1} + E_{K2} + E_{K3}, \end{aligned}$$

where the subscripts "1," "2" and "3" represent the three orthogonal components of $\hat{\mathbf{v}}$ or E_K. Therefore, GED can be written as $E_{G(\alpha)} = \alpha E_P + (1-\alpha)E_K$. GED can revert to the traditional acoustic energy density quantities, as shown in Table I. With properly selected values of α, GED can be optimized for different applications.

For diffuse sound fields excited by a single frequency, E_P, E_{K1}, E_{K2}, and E_{K3} all follow the exponential distribution with a unitary mean value, if they are normalized by their spatial mean values.[18] The normalized E_K and E_T (total energy density) follow the Gamma(3, 1/3) distribution. The distribution for GED is more complicated with the probability density function given by[17]

$$\begin{aligned} f_{E_G}(x) = &\frac{27\alpha^2\left(e^{-3x/(1-\alpha)} - e^{-x/\alpha}\right)}{(1-4\alpha)^3} \\ &+ \frac{27x[x(1-4\alpha) - 2\alpha(1-\alpha)]\,e^{-3x/(1-\alpha)}}{2(1-\alpha)^2(1-4\alpha)^2}. \end{aligned} \quad (2)$$

The relative spatial variance for GED is shown to be

$$\epsilon_G^2 = \frac{1}{3}(4\alpha^2 - 2\alpha + 1), \quad (3)$$

which reaches its minimum value, 1/4, when $\alpha = 1/4$.

A. GED based ANC

For active noise control inside an enclosure, the usual approach taken is to minimize the squared pressure response at an error sensor location by adjusting the complex source strength (both amplitude and phase) of the secondary source. In this section, a mathematical derivation is carried out to find the optimal complex source strength if the GED response is minimized.

Suppose the noise field in an enclosure is excited by a single-tone primary noise source. The acoustic pressure and three particle velocity components at a location $\mathbf{r}$ are known and denoted as $\hat{p}_p(\mathbf{r})$, $\hat{v}_{p1}(\mathbf{r})$, $\hat{v}_{p2}(\mathbf{r})$, and $\hat{v}_{p3}(\mathbf{r})$, respectively. The subscript "p" represents the primary sound field. If a secondary source is introduced in the enclosure, then the superposed GED field can be calculated as

$$\begin{aligned} E_{G(\alpha)}(\mathbf{r}) = &\frac{\alpha}{2\rho_0 c^2}\left(\hat{p}_p(\mathbf{r}) + \hat{p}_s(\mathbf{r})\right)\left(\hat{p}_p(\mathbf{r}) + \hat{p}_s(\mathbf{r})\right)^* \\ &+ \frac{1-\alpha}{2}\rho_0\sum_{l=1}^{3}\left(\hat{v}_{pl}(\mathbf{r}) + \hat{v}_{sl}(\mathbf{r})\right) \\ &\times\left(\hat{v}_{pl}(\mathbf{r}) + \hat{v}_{sl}(\mathbf{r})\right)^*, \end{aligned} \quad (4)$$

where $\hat{p}_s(\mathbf{r})$ and $\hat{v}_{sl}(\mathbf{r})$ represent the pressure and the three components of the particle velocity fields due to the secondary source only. The subscript "s" represents the secondary sound field.

The secondary acoustic pressure and particle velocity fields are usually not known before the control system is turned on. The spatial transfer functions from the secondary source to any field location can be measured and denoted as $\hat{Z}p_s$ for pressure and $\hat{Z}v_{sl}$ for particle velocity. Equation (4) then becomes

$$\begin{aligned} E_{G(\alpha)}(\mathbf{r}) = &\frac{\alpha}{2\rho_0 c^2}[\hat{p}_p(\mathbf{r}) + (\hat{Q}_{sr} + i\hat{Q}_{si})\hat{Z}p_s(\mathbf{r})] \\ &\times[\hat{p}_p(\mathbf{r}) + (\hat{Q}_{sr} + i\hat{Q}_{si})\hat{Z}p_s(\mathbf{r})]^* \\ &+ \frac{1-\alpha}{2}\rho_0\sum_{l=1}^{3}[\hat{v}_{pl}(\mathbf{r}) + (\hat{Q}_{sr} + i\hat{Q}_{si})\hat{Z}v_{sl}(\mathbf{r})] \\ &\times[\hat{v}_{pl}(\mathbf{r}) + (\hat{Q}_{sr} + i\hat{Q}_{si})\hat{Z}v_{sl}(\mathbf{r})]^*, \end{aligned}$$

where $\hat{Q}_{sr}$ and $\hat{Q}_{si}$ represent the real and imaginary parts of the complex secondary source strength, $\hat{Q}_s$.

If one is trying to minimize the GED response at location $\mathbf{r_0}$, the optimal $\hat{Q}_s$ value can be solved for from

$$\begin{cases} \dfrac{\partial E_{G(\alpha)}(\mathbf{r_0})}{\partial \hat{Q}_{sr}} = 0, \\ \dfrac{\partial E_{G(\alpha)}(\mathbf{r_0})}{\partial \hat{Q}_{si}} = 0, \end{cases} \quad (5)$$

and the solution is

$$\hat{Q}_s = \hat{Q}_{sr} + i\hat{Q}_{si} = -\frac{\alpha\hat{p}_p(\mathbf{r_0})\hat{Z}p_s^*(\mathbf{r_0}) + (1-\alpha)\rho_0^2c^2\left[\sum_{l=1}^{3}\hat{v}_{pl}(\mathbf{r_0})\hat{Z}v_{sl}^*(\mathbf{r_0})\right]}{\alpha\hat{Z}p_s(\mathbf{r_0})\hat{Z}p_s^*(\mathbf{r_0}) + (1-\alpha)\rho_0^2c^2\left[\sum_{l=1}^{3}\hat{Z}v_{sl}(\mathbf{r_0})\hat{Z}v_{sl}^*(\mathbf{r_0})\right]}. \quad (6)$$

If the primary sound field is also expressed in terms of the primary source strength, $\hat{Q}_p$, and the spatial transfer functions, $\hat{Z}p_p$ and $\hat{Z}v_{pl}$, then Eq. (6) becomes

$$\hat{Q}_s = -\hat{Q}_p \frac{\alpha\hat{Z}p_p(\mathbf{r_0})\hat{Z}p_s^*(\mathbf{r_0}) + (1-\alpha)\rho_0^2c^2\left[\sum_{l=1}^{3}\hat{Z}v_{pl}(\mathbf{r_0})\hat{Z}v_{sl}^*(\mathbf{r_0})\right]}{\alpha\hat{Z}p_s(\mathbf{r_0})\hat{Z}p_s^*(\mathbf{r_0}) + (1-\alpha)\rho_0^2c^2\left[\sum_{l=1}^{3}\hat{Z}v_{sl}(\mathbf{r_0})\hat{Z}v_{sl}^*(\mathbf{r_0})\right]}. \tag{7}$$

In the low frequency range, the numerical study in Ref. 17 shows that minimizing the $E_{G(1/4)}$ response instead of the total acoustic energy density response may lead to improved active control of the global sound energy in a lightly damped enclosure.

III. ZONE OF QUIET IN A DIFFUSE SOUND FIELD

For a diffuse sound field excited by a pure-tone noise source, global active noise control will generally not be achieved unless the control source is placed within half a wavelength from the primary source.[1] When the control source and the primary source are far away from each other, only local attenuation can be obtained. If the pressure response is minimized at the error sensor location $\mathbf{r_0}$, which is in the far field of both sources, an expression for the spatially averaged mean squared pressure p at the location $\mathbf{r_0}+\Delta\mathbf{r}$ has been derived by Elliot *et al.*,[6] which can be written as

$$\langle\overline{p^2(\mathbf{r_0}+\Delta\mathbf{r})}\rangle = [1-\mathrm{sinc}^2(k\Delta r)](\langle\overline{p_p^2}\rangle + \langle\overline{p_s^2}\rangle), \tag{8}$$

where $\langle\overline{\cdots}\rangle$ denotes the spatial and time average, p_p^2 and p_s^2 represent the squared sound pressure of the primary and the secondary sound fields, respectively, k is the wavenumber, and $\Delta r = |\Delta\mathbf{r}|$. The existence of the sinc function on the right hand side of Eq. (8) is rooted from the spatial cross-correlation of two positions distanced by Δr in a diffuse field.[19] Upon arriving at the preceding expression, it was assumed that the cancellation of the sound pressure response is perfect at the location $\mathbf{r_0}$. If a similar derivation to that in Ref. 6 is carried out but without forcing the perfect cancellation of the sound pressure response, one can derive the following more general expression,

$$\langle\overline{p^2(\mathbf{r_0}+\Delta\mathbf{r})}\rangle = \mathrm{sinc}^2(k\Delta r)\langle\overline{p^2(\mathbf{r_0})}\rangle + [1-\mathrm{sinc}^2(k\Delta r)](\langle\overline{p_p^2}\rangle + \langle\overline{p_s^2}\rangle). \tag{9}$$

Comparing this result to Eq. (8), the term $\mathrm{sinc}^2(k\Delta r)\langle\overline{p^2(\mathbf{r_0})}\rangle$ has been added, which draws the correlation to the squared pressure at the error sensor location. The second term on the right hand side of Eq. (9) dominates the whole expression in the far field of the error sensor ($\Delta r > \lambda/2$) where one has

$$\langle\overline{p^2(\mathbf{r_0}+\Delta\mathbf{r})}\rangle \approx \langle\overline{p_p^2}\rangle + \langle\overline{p_s^2}\rangle. \tag{10}$$

Equation (10) suggests that the far-field sound energy will always be increased after ANC.

If the spatially averaged mean squared pressure after ANC is normalized by the same quantity before ANC, Eq. (9) becomes

$$\frac{\langle\overline{p^2(\mathbf{r_0}+\Delta\mathbf{r})}\rangle}{\langle\overline{p_p^2}\rangle} = \mathrm{sinc}^2(k\Delta r)\frac{\langle\overline{p^2(\mathbf{r_0})}\rangle}{\langle\overline{p_p^2}\rangle} + [1-\mathrm{sinc}^2(k\Delta r)]\left(1+\frac{\langle\overline{p_s^2}\rangle}{\langle\overline{p_p^2}\rangle}\right). \tag{11}$$

The fraction in the first term of the right-hand side of Eq. (11) represents the normalized spatially averaged mean squared pressure at the error sensor location. If the GED response is minimized, this term can be calculated in the frequency domain as

$$\frac{\langle\overline{p^2(\mathbf{r_0})}\rangle}{\langle\overline{p_p^2}\rangle} = \frac{\langle[\hat{p}_p(\mathbf{r_0})+\hat{p}_s(\mathbf{r_0})][\hat{p}_p(\mathbf{r_0})+\hat{p}_s(\mathbf{r_0})]^*\rangle}{\langle\hat{p}_p\hat{p}_p^*\rangle} = \frac{\langle[\hat{Q}_p\hat{Z}p_p(\mathbf{r_0})+\hat{Q}_s\hat{Z}p_s(\mathbf{r_0})][\hat{Q}_p\hat{Z}p_p(\mathbf{r_0})+\hat{Q}_s\hat{Z}p_s(\mathbf{r_0})]^*\rangle}{\langle\hat{Q}_p\hat{Z}p_p\hat{Q}_p^*\hat{Z}p_p^*\rangle}$$
$$= \frac{\langle[\hat{Z}p_p(\mathbf{r_0})+(\hat{Q}_s/\hat{Q}_p)\hat{Z}p_s(\mathbf{r_0})][\hat{Z}p_p(\mathbf{r_0})+(\hat{Q}_s/\hat{Q}_p)\hat{Z}p_s(\mathbf{r_0})]^*\rangle}{\langle\hat{Z}p_p\hat{Z}p_p^*\rangle}, \tag{12}$$

where Q_s can be found in Eq. (7). The substitution of Eq. (7) into Eq. (12) makes the expression rather complicated. However, given that $\hat{Z}p_p$, $\hat{Z}p_s$, $\hat{Z}v_{pl}$, and $\hat{Z}v_{sl}$ are all mutually independent variables with mean values being equal to zero, and $\langle\hat{Z}v_{pl}\hat{Z}v_{pl}^*\rangle/\langle\hat{Z}p_p\hat{Z}p_p^*\rangle = 1/3$,[18] the expression can be simplified to

$$\frac{\langle\overline{p^2(\mathbf{r_0})}\rangle}{\langle\overline{p_p^2}\rangle} = \frac{(1-\alpha)^2}{3}\left\langle\frac{E_{PZs}E_{KZs}+3E_{KZs}^2}{[\alpha E_{PZs}+(1-\alpha)E_{KZs}]^2}\right\rangle, \tag{13}$$

where $E_{PZs} = \hat{Z}p_s\hat{Z}p_s^*$ and $E_{KZs} = \rho_0^2c^2\sum_{l=1}^{3}\hat{Z}v_{sl}\hat{Z}v_{sl}^*$. E_{PZs} and E_{KZs} are independent random variables and have the same mean value, $\langle E_{PZs}\rangle = \langle E_{KZs}\rangle = \mu_Z$. In addition,

E_{PZs}/μ_Z is distributed as $Gamma(1, 1)$, and E_{KZs}/μ_Z is distributed as $Gamma(3, 1/3)$. Therefore Eq. (13) can be expressed as

$$\begin{aligned}\frac{\overline{\langle p^2(\mathbf{r_0})\rangle}}{\langle \overline{p_p^2}\rangle} &= \frac{(1-\alpha)^2}{3}\left\langle \frac{E_{PZs}E_{KZs}+3E_{KZs}^2}{\left[\alpha E_{PZs}+(1-\alpha)E_{KZs}\right]^2}\right\rangle \\ &= \frac{(1-\alpha)^2}{3}\left\langle \frac{E_{PZs}E_{KZs}/\mu_Z^2+3E_{KZs}^2/\mu_Z^2}{\left[\alpha E_{PZs}/\mu_Z+(1-\alpha)E_{KZs}/\mu_Z\right]^2}\right\rangle \\ &= \frac{(1-\alpha)^2}{3}\int_0^\infty\int_0^\infty \frac{xy+3y^2}{\left[\alpha x+(1-\alpha)y\right]^2}\cdot e^{-x} \\ &\quad\times\frac{27y^2e^{-3y}}{2}dxdy. \end{aligned} \tag{14}$$

The integration in Eq. (14) is still involved. However, it is possible to obtain some important properties of $\langle p^2(\mathbf{r_0})\rangle/\langle \overline{p_p^2}\rangle$ fairly easily. First, $\langle p^2(\mathbf{r_0})\rangle/\langle \overline{p_p^2}\rangle$ is monotonically decreasing for $0 \le \alpha \le 1$, which can be proven by showing that its derivative with respect to α is always negative. When α is equal to one, GED reverts to the potential energy density (or squared pressure). Therefore it is not surprising that the squared pressure at the error sensor location reaches its minimum value, zero, when squared pressure is minimized.

When $\alpha = 0$, which is equivalent to minimizing the squared particle velocity, Eq. (14) is relatively easier to evaluate and becomes

$$\left.\frac{\overline{\langle p^2(\mathbf{r_0})\rangle}}{\langle \overline{p_p^2}\rangle}\right|_{\alpha=0} = \frac{1}{3}\int_0^\infty\int_0^\infty \frac{x+3y}{y}\cdot e^{-x}\cdot\frac{27y^2e^{-3y}}{2}dxdy = \frac{3}{2}, \tag{15}$$

which indicates an amplified pressure field at the error sensor location. Another easily integrated case is when $\alpha = 1/4$, resulting in

$$\left.\frac{\overline{\langle p^2(\mathbf{r_0})\rangle}}{\langle \overline{p_p^2}\rangle}\right|_{\alpha=1/4} = 3\int_0^\infty\int_0^\infty \frac{y}{x+3y}\cdot e^{-x}\cdot\frac{27y^2e^{-3y}}{2}dxdy = \frac{3}{4}. \tag{16}$$

A numerical evaluation of Eq. (14) for $0 \le \alpha \le 1$ is plotted in Fig. 1 on a logarithmic scale.

To reduce the squared pressure at the error sensor location to at least 10 dB lower than the averaged primary squared pressure, α needs to be greater than about 0.88. When α is equal to 0.6, about 5 dB reduction can be achieved.

In a similar manner, the term, $\langle \overline{p_s^2}\rangle$, in Eq. (9) and Eq. (11) can be calculated as follows:

$$\begin{aligned}\langle \overline{p_s^2}\rangle &= \langle \hat{Q}_s(\mathbf{r_0})\hat{Z}p_s(\mathbf{r})\hat{Q}_s^*(\mathbf{r_0})\hat{Z}p_s^*(\mathbf{r})\rangle \\ &= \langle \hat{Q}_s\hat{Q}_s^*\rangle\langle \hat{Z}p_s\hat{Z}p_s^*\rangle. \end{aligned} \tag{17}$$

For the frequency range well above the Schroeder frequency, $\langle \hat{Z}p_s\hat{Z}p_s^*\rangle$ is equal to $\langle \hat{Z}p_p\hat{Z}p_p^*\rangle$; therefore

$$\begin{aligned}\langle \hat{Q}_s\hat{Q}_s^*\rangle\langle \hat{Z}p_s\hat{Z}p_s^*\rangle &= \frac{\langle \hat{Q}_s\hat{Q}_s^*\rangle}{\hat{Q}_p\hat{Q}_p^*}\cdot\hat{Q}_p\hat{Q}_p^*\langle \hat{Z}p_p\hat{Z}p_p^*\rangle \\ &= \left\langle \frac{\hat{Q}_s}{\hat{Q}_p}\frac{\hat{Q}_s^*}{\hat{Q}_p^*}\right\rangle\langle \overline{p_p^2}\rangle. \end{aligned} \tag{18}$$

By substituting Eq. (7) and following the considerations to derive Eq. (14), the averaged ratio of secondary source strength to the primary source strength can be calculated as

$$\begin{aligned}\left\langle \frac{\hat{Q}_s}{\hat{Q}_p}\frac{\hat{Q}_s^*}{\hat{Q}_p^*}\right\rangle &= \left\langle \frac{3\alpha^2E_{PZs}+(1-\alpha)^2E_{KZs}}{3\left[\alpha E_{PZs}+(1-\alpha)E_{KZs}\right]^2}\right\rangle \\ &= \int_0^\infty\int_0^\infty \frac{3\alpha^2x+(1-\alpha)^2y}{3\left[\alpha x+(1-\alpha)y\right]^2}\cdot e^{-x}\cdot\frac{27y^2e^{-3y}}{2}dxdy. \end{aligned} \tag{19}$$

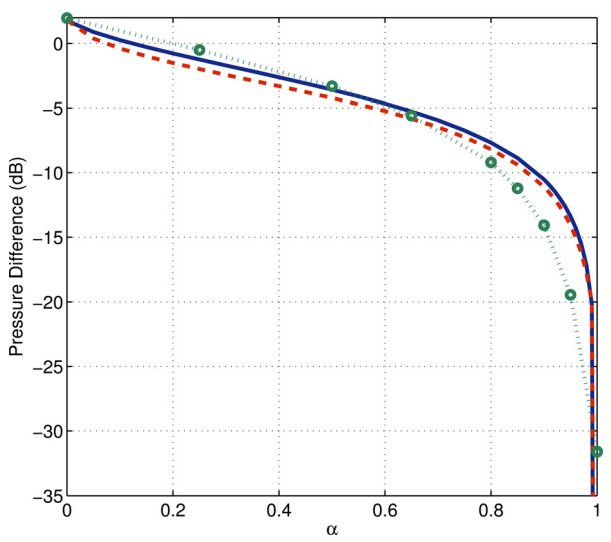

FIG. 1. (Color online) Ratio of the spatially averaged mean squared pressure at the error sensor location when GED is minimized to the averaged mean square pressure of the entire primary sound field, $10\log_{10}(\langle p^2(\mathbf{r_0})\rangle/\langle \overline{p_p^2}\rangle)$. —, Eq. (14); −−, computer simulation based on the example discussed in Sec. IV; ·· ○ ··, experimental results discussed in Sec. VI.

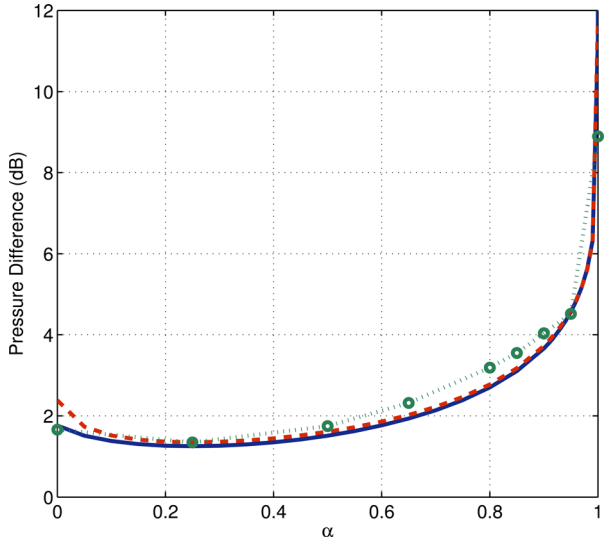

FIG. 2. (Color online) Ratio of the spatially averaged mean squared pressure at the remote location when GED is minimized to the averaged mean square pressure of the entire primary sound field, $10\log_{10}(1+\langle \overline{p_s^2}\rangle/\langle \overline{p_p^2}\rangle)$. —, Eq. (20); −−, computer simulation based on the example discussed in Sec. IV; ·· ○ ··, experimental results discussed in Sec. VI.

Substituting Eqs. (18) and (19) into Eq. (17) leads to

$$\frac{\langle \overline{p_s^2} \rangle}{\langle \overline{p_p^2} \rangle} = \left\langle \frac{\hat{Q}_s}{\hat{Q}_p} \frac{\hat{Q}_s^*}{\hat{Q}_p^*} \right\rangle = \int_0^\infty \int_0^\infty \frac{3\alpha^2 x + (1-\alpha)^2 y}{3\left[\alpha x + (1-\alpha) y\right]^2} \cdot e^{-x} \cdot \frac{27 y^2 e^{-3y}}{2} dx dy. \tag{20}$$

It can be shown that the source strength ratio has a minimum value of 1/3 when $\alpha = 1/4$. In addition, the ratio approaches infinity when $\alpha = 0$, which was originally derived theoretically in Ref. 6. In that reference, Elliott *et al.* assigned a value of 3 for this situation based on a numerical study due to the consideration that the secondary source power may not reach infinity in reality. Those authors, however, noticed the lack of repeatability in the numerical simulation results. As is found later in this paper, it was found numerically and experimentally that the averaged sound power ratio can be very high and cause an increase of more than 12 dB in the far field of the error sensor when $\alpha \to 1$. Combining Eqs. (17)–(20), the far field squared pressure value $\langle \overline{p_p^2} \rangle + \langle \overline{p_s^2} \rangle$ can be evaluated numerically and is plotted in Fig. 2.

The value of α has a different impact on the near field and the far field regions of the sound pressure after ANC is implemented. To maximize the noise reduction at the error sensor location, α needs to be equal to one. On the other hand, however, the value of $\alpha = 1$ should be avoided due to the possible extremely high secondary source strength and significant amplification introduced in the far field. The averaged sound pressure level around the error sensor is plotted in Fig. 3 for values of α being 0.999999, 0.95, 0.85, 0.5, and 0.25. Because of the divergent nature of minimizing squared pressure, the value 0.999999 is used instead of one. One can observe from the plot that the 10 dB "quiet zone" for minimizing pressure is noticeably smaller than the generally reported volume—a sphere with diameter being one-tenth of the wavelength. This

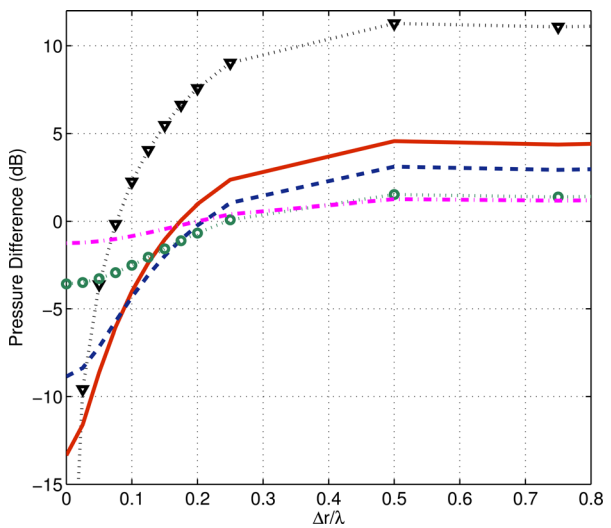

FIG. 3. (Color online) Spatially averaged mean square pressure in the near field of the error sensor when GED is minimized. Equation (11) is evaluated numerically and $10\log_{10}(\langle \overline{p^2(\mathbf{r_0}+\Delta\mathbf{r})} \rangle / \langle \overline{p_p^2} \rangle)$ is plotted. ·· △ ··, $E_{G(1)}$ (E_P); —, $E_{G(0.95)}$; − −, $E_{G(0.85)}$; ·· ○ ··, $E_{G(0.5)}$; − · −, $E_{G(0.25)}$.

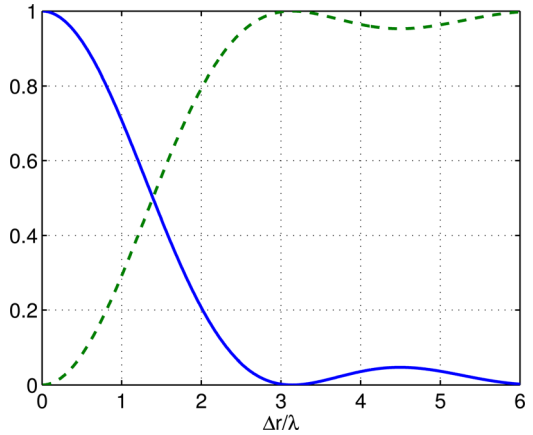

FIG. 4. (Color online) Plot of the squared sinc function. —, $\mathrm{sinc}^2(k\Delta r)$; − −, $1 - \mathrm{sinc}^2(k\Delta r)$.

size, however, can be reached by setting $\alpha = 0.95$. If a controlled volume of 5 dB reduction is desired, a value of α in the range of approximately 0.85 to 0.95 can provide a quiet zone with the diameter being around one-fifth of the wavelength. If the general quiet zone, defined as the region where the noise is reduced, is considered, it has a diameter of around two-fifths of the wavelength for $\alpha < 0.85$, which is noticeably larger than for $\alpha \approx 1$. In the far field, greater than about half a wavelength away from the error sensor, the averaged pressure field is much lower for $\alpha < 0.95$ than for $\alpha \approx 1$. The theoretical minimum average far field pressure can be achieved when $\alpha = 0.25$. However, for this case the largest noise reduction is less than 5 dB, as is also the case for $\alpha = 0.5$.

To shed some physical insights as to why the GED based approach produces an enlarged quiet zone, Eq. (11) needs to be re-visited. Figure 4 compares the functions $\mathrm{sinc}^2(k\Delta r)$ and $1 - \mathrm{sinc}^2(k\Delta r)$ that lead the two terms on the right-hand side of the equation. In the region very close to the error sensor location ($k\Delta r \ll 1$), $[1 - \mathrm{sinc}^2(k\Delta r)] \to 0$; therefore the first term on the right-hand side of the equation dominates. However, for the the desired cases where $(\langle \overline{p^2(\mathbf{r_0})} \rangle / \langle \overline{p_p^2} \rangle) \ll 1$, the second term starts to dominate the response very quickly as Δr increases, and the sound pressure pattern in the near field of the error sensor location is actually mostly influenced by the shape of the function $[1 - \mathrm{sinc}^2(k\Delta r)]$. For the response to rise slowly, the multiplier to that function, $(1 + \langle \overline{p_s^2} \rangle / \langle \overline{p_p^2} \rangle)$, needs to be small. However, when the squared pressure is minimized, the multiplier term is extremely large, which is due to the ill condition that occurs when the inverse is taken on a random variable (squared pressure) following the exponential distribution. As a result, $\langle \overline{p_s^2} \rangle / \langle \overline{p_p^2} \rangle$ is very large, and the level of the sound pressure field increases very fast as one moves away from the error sensor location. Adding the squared particle velocity, even with a small weighting factor, helps avoid the ill condition, which results in a much smaller value of $\langle \overline{p_s^2} \rangle / \langle \overline{p_p^2} \rangle$ [see Fig. 2] and thus an enlarged quiet zone.

IV. NUMERICAL SIMULATION

Computer simulations were carried out to verify the theoretical derivations in Sec. III. Inside a lightly damped room

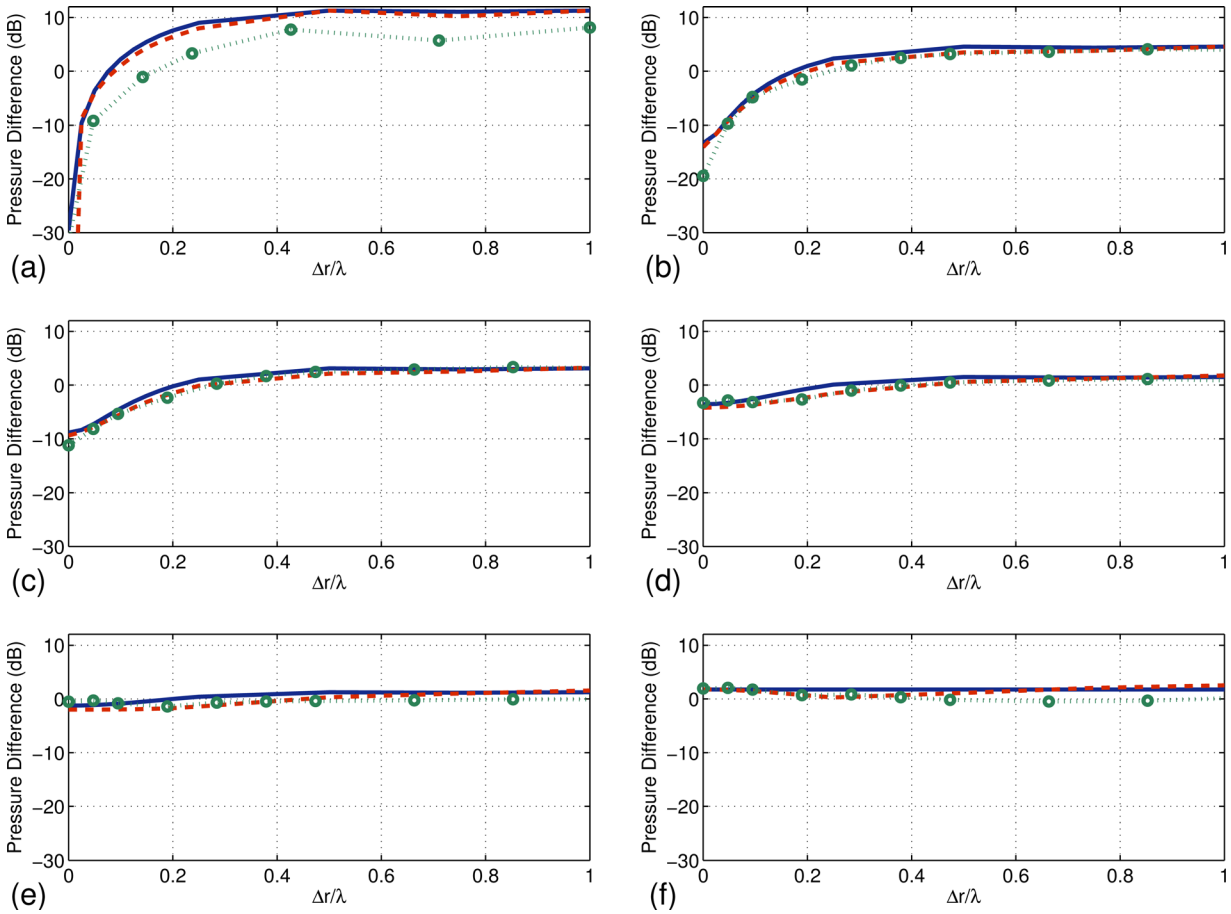

FIG. 5. (Color online) Averaged mean square pressure in the near field of the error sensor when GED is minimized. Comparisons are made among the theoretical predictions, the numericial simulation results and the experimental results for (a) E_P, (b) $E_{G(0.95)}$, (c) $E_{G(0.85)}$, (d) $E_{G(0.5)}$, (e) $E_{G(0.25)}$, and (f) E_K. —, Eq. (14); − −, computer simulation based on the example discussed in Sec. IV; ·· ○ ··, experimental results discussed in Sec. VI.

(dimensions: $2e\,\mathrm{m} \times 2\pi\,\mathrm{m} \times 6\,\mathrm{m}$), the GED field of the primary point source is minimized at an error sensor location by one remotely placed secondary point source. The room has a uniform wall impedance, $z = (50 + 100i)\rho_0 c$, with the Schroeder frequency being 310 Hz. The error sensor is placed at 3/8 of the length along one diagonal line of the room. The primary and secondary source locations are randomly chosen within the region that is at least two wavelengths from the error sensor and the boundaries. Sound fields for a point source at 200 such selected random locations are computed with a hybrid modal expansion model[20] at 800 Hz, which is well above the Schroeder frequency of the room to meet the diffuse field condition. The hybrid modal expansion model was demonstrated to be more accurate and converge faster than the classical modal expansion for both the sound pressure field and the particle velocity field.[20] Based on these 200 source locations, a search was carried out to look for two sources that were at least ten wavelengths away from each other. More than 4000 such pairs were found, and with each pair, one source was randomly selected to serve as the primary source while the other one was used as the secondary source. Because the complex source strengths were set to be unity, the pressure and particle velocity fields computed correspond to the spatial transfer functions. The secondary source strength required to minimize the GED response at the error sensor location can be calculated using Eq. (7). The controlled sound field is then computed by superposing the primary and secondary fields. The averaged squared pressure (over 4000 trials) at the error sensor location and at a remote region has been plotted in Figs. 1 and 2 to be compared with the analytical predictions and the experimental results. The averaged near field results are plotted in Fig. 5 to compare with the analytical and the experimental results. All the numerical simulations agree well with theoretical results.

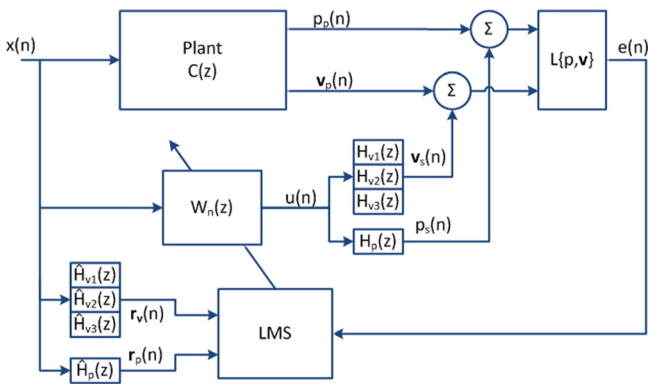

FIG. 6. (Color online) Block diagram of the energy-based filtered-x LMS algorithm.

V. A FILTERED-X LMS ALGORITHM FOR GED

The ANC algorithm utilized in this study is based on a version of the widely used adaptive filtered-x LMS

algorithm, which has been modified for the minimization of the acoustic energy-based quantities.[21] A block diagram representing the ANC algorithm is shown in Fig. 6. In this figure, $p_p(n)$, $\mathbf{v}_p(n)$, $p_s(n)$, and $\mathbf{v}_s(n)$ represent the pressure and particle velocity at the error sensor due to the primary and secondary source, respectively. Here, n denotes a discrete-time index. W_n in the diagram represents the adaptive active control filter, while H_{vi} and H_p denote the transfer functions representing the secondary path for the particle velocity and pressure, respectively. The estimated secondary path filters are denoted as $\hat{H}_{vi}$ and $\hat{H}_p$, with the resulting output signal being $\mathbf{r}_\mathbf{v}(n)$ and $\mathbf{r}_p(n)$, respectively. This block diagram is essentially identical to the one introduced by Ref. 21. The only difference is the function $\mathrm{L}\{p, \mathbf{v}\}$ in the diagram is now representing a procedure of computing the square root of GED instead of the ED. The control filter update equation thus includes the variable α and reads

$$\mathbf{w}(n+1) = \mathbf{w}(n) - \mu_X \left[\frac{\alpha}{\rho_0 c^2} p(n)\mathbf{r}_p + (1-\alpha)\rho_0 \sum_{l=1}^{3} v_i(n)\mathbf{r}_{vi} \right], \tag{21}$$

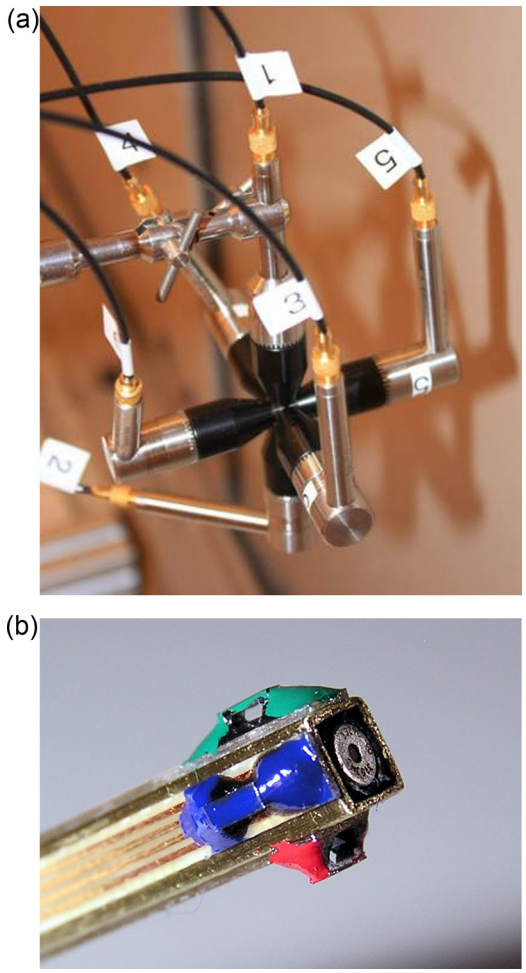

FIG. 7. (Color online) Examples of GED probes. (a) A microphone gradient GED probe; (b) the Ultimate Sound Probe (USP). A USP probe consists of three orthogonal particle velocity components (the Micoflown sensors) and one pressure component (a microphone).

where μ_X is the convergence parameter. With no surprise, this expression can revert to the active control filter update equations for minimizing the squared pressure, squared velocity, or total acoustic energy density by choosing the appropriate corresponding value for α. Of note is the fact that an existing ANC system based on minimizing ED can be very easily modified to minimize E_G instead.

VI. EXPERIMENTAL STUDY

An experimental study was carried out in a reverberation chamber that has dimensions of 4.96 m × 5.89 m × 6.98 m (a volume of 204 m^3) and is incorporated with stationary diffusers. The Schroeder frequency for this chamber is 410 Hz. The filtered-x LMS algorithm discussed in Sec. V was implemented in a real-time system powered by a TI TMS320C6713 DSP processor.[22] The sampling frequency of the system was set to be 4000 Hz. The adaptive control filter and secondary path filters are all finite impulse response (FIR) filters with 8 coefficients. The step size, μ_X was set to be 10^{-10}.

A pressure microphone gradient probe served as the error sensor, which is shown in Fig. 7(a). The probe consists of three pairs of phase matched 1/2-inch microphones manufactured by G.R.A.S. The microphone pairs are placed perpendicular to each other, so three orthogonal particle velocity components can be estimated based on the pressure gradient.[23,24] The spacing between microphones in each pair is 5 cm, which allows good accuracy in the frequency range below 1000 Hz. The acoustic pressure was estimated by averaging the pressure signals from all six microphones in the probe. The GED can thus be estimated using Eq. (1). Because the error of the sound pressure estimation introduced by the averaging of six microphones can greatly affect the ANC performance when $E_{G(1)}$ or squared pressure is minimized, a G.R.A.S 1/2-inch free-field microphone with a diffuse cap was used for this case instead of the GED probe.

One loudspeaker driven by a signal generator outputting a 650 Hz pure-tone signal served as the primary source. The output of the signal generator was also connected to the ANC system, serving as the reference signal. Another identical loudspeaker was used as the secondary source. The secondary path filters were estimated offline at 650 Hz only using a multi-channel Wiener filter approach.[22]

Twenty tests were carried out. The error sensors were located near the center of the chamber and the location remained constant. The locations of the two sources were chosen randomly for each test, but the sources were at least two wavelengths from the boundaries and the error sensor. The distance between the two sources was at least 5 wavelengths away from each other. The sound pressure fields both without and with control were sampled at different distances from the error sensor. The averaged difference between the sound pressure fields with control on and off are calculated and compared with the theoretical and simulation results in Fig. 5 with respect to the distance from the error sensor for some specific values of α. The far field pressure field was sampled with six far field microphones. The difference between the averaged far field squared pressure values for control on and off are plotted in Fig. 2 as a function of α.

The experimental results and the theoretical and computer simulation results are in good agreement.

A. Discussion

The pressure microphone gradient probe used in the experimental study is comparable in size comparing to the quiet zone generated for the 650 Hz pure-tone sound. Although it is appropriate here to serve the purpose of verifying the theoretical results, it may not be desired in practice. In a real-world ANC application, other GED capable probes with much smaller physical size could be considered. One example is the Microflown Ultimate Sound Probe as shown in Fig. 7(b),[25,26] the size of which is similar to the size of a 1/2-inch microphone. To further reduce the effect of the physical size of the probes, the virtual error sensor technology developed for ED based ANC[14] can be easily adopted for GED-based ANC at the cost of additional measurements of the transfer functions between the physical sensor locations and the virtual sensor locations.

VII. CONCLUSIONS

GED-based active noise control is studied in this paper for diffuse sound fields. The averaged zone of quiet in the near field of the error sensor was derived theoretically and verified by a numerical simulation. Compared to minimizing squared pressure response, by varying the value of α of GED, one can increase the size of the general zone of quiet by as much as three times. As a trade off, the maximum attenuation may decrease to around 1.25 dB. By choosing appropriate values of α, one can maximize the volume of the quiet zone and at the same time obtain the desired attenuation. For example, if a 10 dB zone of quiet is required, a value of 0.95 may be assigned to α. When an attenuation of 5 dB is desired, a value of 0.85 should be assigned to α. In the far field of the error sensor, there is usually an amplification of the squared pressure. However, it was shown in this work that by minimizing the GED response with $\alpha < 1$, the amplification in the far field can be dramatically reduced.

The filtered-x LMS algorithm developed for the ED-based ANC was adapted in this paper for GED-based ANC. In practice, very minimal effort is needed to modify an existing ED-based ANC system to a GED-based ANC system.

The experimental study conducted in a reverberation chamber largely confirmed the theoretical results derived in the paper.

[1]P. A. Nelson, A. R. D. Curtis, S. J. Elliott, and A. J. Bullmore, "The active minimization of harmonic enclosed sound fields. I. Theory," J. Sound Vib. **117**, 1–13 (1987).

[2]A. J. Bullmore, P. A. Nelson, A. R. D. Curtis, and S. J. Elliott, "The active minimization of harmonic enclosed sound fields. II. A computer simulation," J. Sound Vib. **117**, 15–33 (1987).

[3]S. J. Elliott, A. R. D. Curtis, A. J. Bullmore, and P. A. Nelson, "Active minimization of harmonic enclosed sound fields. III. Experimental verification," J. Sound Vib. **117**, 35–58 (1987).

[4]D.-Y. Maa, "Sound field in a room and its active noise control," Appl. Acoust. **41**, 113–126 (1994).

[5]P. Nelson and S. Elliott, *Active Control of Sound* (Academic, London, 1993), Chap. 10.

[6]S. J. Elliott, P. Joseph, A. J. Bullmore, and P. A. Nelson, "Active cancellation at a point in a pure tone diffuse sound field," J. Sound Vib. **120**, 183–189 (1988).

[7]P. Joseph, S. J. Elliott, and P. A. Nelson, "Near field zones of quiet," J. Sound Vib. **172**, 605–627 (1994).

[8]P. Joseph, S. J. Elliott, and P. A. Nelson, "Statistical aspects of active control in harmonic enclosed sound fields," J. Sound Vib. **172**, 629–655 (1994).

[9]S. J. Elliott and J. Garcia-Bonito, "Active cancellation of pressure and pressure gradient in a diffuse sound field," J. Sound Vib. **186**, 696–704 (1995).

[10]J. Garcia-Bonito and S. J. Elliott, "Local active control of diffuse sound fields," J. Acoust. Soc. Am. **98**, 1017–1024 (1995).

[11]J. Garcia-Bonito and S. J. Elliott, "Active cancellation of acoustic pressure and particle velocity in the near field of a source," J. Sound Vib. **221**, 85–116 (1999).

[12]J. Garcia-Bonito, S. J. Elliott, and C. Boucher, "Generation of zones of quiet using a virtual microphone arrangement," J. Acoust. Soc. Am. **101**, 3498–3516 (1997).

[13]D. J. Moreau, J. Ghan, B. S. Cazzolato, and A. C. Zander, "Active noise control in a pure tone diffuse sound field using virtual sensing," J. Acoust. Soc. Am. **125**, 3742–3755 (2009).

[14]D. J. Moreau, J. Ghan, B. S. Cazzolato, and A. C. Zander, "Active noise control at a virtual acoustic energy density sensor in a three-dimensional sound field," in *Proceedings of the 20th International Congress on Acoustics*, Sydney, Australia (2010).

[15]J. W. Parkins, "Active minimization of energy density in a three-dimensional enclosure," Ph.D. dissertation, Pennsylvania State University, State College, PA, 1998.

[16]J. W. Parkins, S. D. Sommerfeldt, and J. Tichy, "Narrowband and broadband active control in an enclosure using the acoustic energy density," J. Acoust. Soc. Am. **108**, 192–203 (2000).

[17]B. Xu, S. D. Sommerfeldt, and T. W. Leishman, "Generalized acoustic energy density," J. Acoust. Soc. Am. **130**, 1370–1380 (2011).

[18]F. Jacobsen, "The diffuse sound field: Statistical considerations concerning the reverberant field in the steady state," Technical Report, Technical University of Denmark (1979).

[19]R. K. Cook, R. V. Waterhouse, R. D. Berendt, S. Edelman, and J. M. C. Thompson, "Measurement of correlation coefficients in reverberant sound fields," J. Acoust. Soc. Am. **27**, 1072–1077 (1955).

[20]B. Xu and S. D. Sommerfeldt, "A hybrid modal analysis for enclosed sound fields," J. Acoust. Soc. Am. **128**, 2857–2867 (2010).

[21]S. D. Sommerfeldt and P. J. Nashif, "An adaptive filtered-x algorithm for energy-based active control," J. Acoust. Soc. Am. **96**, 300–306 (1994).

[22]B. M. Faber, "Active minimization of acoustic energy density in a mock tractor cab," M.S. thesis, Brigham Young University, Provo, UT, 2004.

[23]I. Wolff and F. Massa, "Use of pressure gradient microphones for acoustical measurements," J. Acoust. Soc. Am. **4**, 217–234 (1933).

[24]F. J. Fahy, "Measurement of the acoustic intensity using the cross-spectral density of two microphone signals," J. Acoust. Soc. Am. **62**, 1057–1059 (1977).

[25]H.-E. de Bree, P. Leussink, T. Korthorst, H. Jansen, T. S. J. Lammerink, and M. Elwenspoek, "The μ-fown: A novel device for measuring acoustic flows," Sensors Actuators A **54**, 552–557 (1996).

[26]T. G. H. Basten and H.-E. de Bree, "Full bandwidth calibration procedure for acoustic probes containing a pressure and particle velocity sensor," J. Acoust. Soc. Am. **127**, 264–270 (2010).